10

Magnetism of Transition Metal Doped GaN Nanostructures

Q. Wang and P. Jena

Physics Department, Virginia Commonwealth University, Richmond, VA 23284, USA

10.1 INTRODUCTION

The current information revolution puts increasing demand for faster, smaller, low power and high storage capacity devices for processing of information. Spin-based electronics, commonly referred to as spintronics, is an emergent technology that innovatively manipulates the spin and charge states of electrons to carry and store information. Since the spintronic devices are smaller, more versatile and robust than the traditional electronic devices, they have the potential to fundamentally alter the electronics industry.

In order to make a spintronics device, the primary requirement is to have a system that can generate a current of spin polarized electrons, and a system that is sensitive to the spin polarization of the electrons. The simplest method of generating a spin polarized current is to inject the current through a giant magnetoresistance (GMR) device. A typical GMR

Porous Silicon Carbide and Gallium Nitride: Epitaxy, Catalysis, and Biotechnology Applications
Edited by Randall M. Feenstra and Colin E.C. Wood

device consists of at least two layers of FM materials separated by a spacer layer. When the two magnetization vectors of the FM layers are aligned, an electrical current will flow freely, whereas if the magnetization vectors are antiparrallel then the resistance of the system is higher. So, spintronic materials have the basic requirements – high spin polarization and long spin relaxation time. Realization of functional spintronic devices requires the materials to be FM at operational temperature.

Dilute magnetic semiconductors (DMSs) are good candidates for spintronic devices. DMS materials are based on nonmagnetic wide band gap semiconductors such as GaN and ZnO where several atomic % of Ga or Zn atoms are substituted by transition metal atoms, such as Mn, Cr, and Fe. At low dopant concentration, crystal structure of the host semiconductor material is unchanged and the DMS materials possess the properties of not only a FM material, but also that of the semiconductor host. Among the various DMSs, transition metal doped GaN materials are particularly interesting and are regarded as prime candidates for spintronics applications since GaN is a direct wide band gap semiconductor with high thermal, chemical, and mechanical stability. Moreover, Mn and Cr atoms have high magnetic moments.

Since the discovery of ferromagnetism in (Ga,Mn)As [1] and the subsequent theoretical prediction [2] that Mn-doped GaN can be FM at or above room temperature, numerous experimental attempts have been made to synthesize this promising DMS material [3–19]. However, the results have been rather confusing. Not only the reported Curie temperatures [3–14] vary over a wide range (10–945 K), but also it is uncertain whether the ground state of (Ga, Mn)N is FM or antiferromagnetic (AFM) [15–21]. The nature and origin of the magnetic coupling in this material continue to be a hotly debated issue. The mechanism for the observed magnetic behavior is complex and appears to depend on a number of factors, including the sample preparation conditions, presence of defects, Mn–Mn separation, and carrier density and type. An understanding of the controversy between FM and AFM is both important and challenging [20, 21]. However, several groups have recently reported above room temperature ferromagnetism for (Ga, Cr)N [22–25] in both bulk and thin film forms. A fundamental understanding of the magnetic coupling between Mn atoms and Cr atoms in GaN is crucial for the development of spintronics devices from these DMSs.

To understand the origin of magnetism in Mn- and Cr-doped GaN, we have performed extensive theoretical calculations on (Ga,Mn)N and (Ga,Cr)N systems from zero-dimensional clusters to one-dimensional nanowires, nanotubes, and nanoholes; two-dimensional surfaces and

thin films; and three-dimensional crystals. These extensive studies enable us to unravel how the inter-atomic distance, local coordination, and dimensionality of a material control not only the magnetic moments of atoms but also the coupling between them. This understanding is also helpful in designing new DMSs such as Mn-doped nanoporous GaN. Note that a nanopore is characterized by large surface area whose orientation can differ from those of bulk surfaces. In the following we discuss these results by concentrating on GaN host.

10.2 Mn-DOPED GaN CRYSTAL

We begin with the study of the electronic structure, energetics and magnetism of Mn-doped GaN crystal. Pure GaN normally crystallizes into the hexagonal wurtzite structure, which consists of Ga and N planes stacked alternatively along the *c*-axis with the Ga and N ions tetrahedrally coordinated. The lattice constants are $a = b = 3.189$ Å, and $c = 5.185$ Å, with a space group $P6_3mc$ (no. 186). We first generated a ($2 \times 2 \times 2$) supercell to explore the electronic structure and magnetic properties of bulk $Ga_{1-x}Mn_xN$, which consists of 16 formula units of GaN. To study the magnetic coupling between the Mn atoms, it is necessary to replace at least two Ga atoms with Mn in the supercell. The Mn–Mn distance and Mn-N-Mn bond angles were varied by replacing the Ga atoms at different sites, until the total energy reached a minimum. To study the influence of the surpercell size and the Mn doping concentration on the magnetic coupling, the calculations were repeated by constructing a ($3 \times 3 \times 2$) supercell. Theoretical calculations were carried out by using the density functional formalism [26]. Exchange and correlation effects were incorporated using the PW91 functional [27] for the generalized gradient approximation (GGA). The electronic structure, total energies and magnetic properties were calculated using a plane-wave basis set with the projector augmented wave (PAW) method [28] as implemented in the Vienna *Ab initio* Simulation Package (VASP) [29]. The cutoff energy was set at 330 eV for the plane-wave basis (the default of maximum cut-off energy is 269.89 eV). In all calculations, self-consistency was achieved with a tolerance in the total energy of at least 1 meV. Hellman–Feynman force components on each ion in the supercells converged to 1 meV $Å^{-1}$.

We first discuss the results based on a GaN ($2 \times 2 \times 2$) supercell having wurtzite structure. Two Ga atoms in this supercell were replaced with Mn atoms, corresponding to a $Ga_{14}Mn_2N_{16}$ supercell and a 12.5 % Mn doping concentration. Note that in recent experiments Mn concentration

from 3 to 15% have been investigated. Since it is a priori not clear which of the two Ga sites Mn atoms would prefer to substitute, we carried out an extensive search for all possible geometrical configurations. In each case, the geometry (ionic coordinates and *c/a* ratio) was fully optimized without any symmetry constraint. The total energies, electronic structure and magnetic moments located at each Mn atom were calculated self-consistently for different spin alignments (FM and AFM) for each of these configurations. The *k*-point convergence was achieved with ($6 \times 6 \times 6$) Monkhorst–Pack grid [30].

We found that without structure optimization the coupling between these two Mn atoms is FM as predicted by previous studies [31–35]. The FM state lies 0.053 eV in energy lower than the AFM state. When the geometry is fully optimized (including ionic coordinates and *c/a* ratio), the FM state is still lower in energy than the AFM state by 0.077 eV. The relaxed Mn–N bond length is found to be 1.99 Å, which is in good agreement with the experimental value of 2.01 ± 0.03 Å [36]. Thus the geometry optimization in the bulk does not alter the preferred magnetic coupling.

The calculations were repeated using a ($3 \times 3 \times 2$) supercell that corresponds to 72 atoms ($Ga_{36}N_{36}$). With two Ga atoms in this supercell replaced with Mn at different sites, the resulting Mn doping concentration corresponds to 5.6 %. The ($5 \times 5 \times 5$) Monkhorst–Pack *k*-point mesh was used. The calculated results were found to be nearly the same as that given for the smaller supercell, namely, the ground state in Mn-doped GaN bulk is FM and lies 0.10 eV lower in energy than the AFM state. The Mn–N bond length is 1.98 Å. Thus, it is clear that the FM coupling between Mn atoms in bulk GaN is independent of the Mn concentration or supercell size.

10.3 Mn-DOPED GaN THIN FILMS

The above discussion does not explain why in certain experiments the coupling between Mn atoms exhibits antiferromagnetism or spin glass behavior. We note that most of these experiments involve thin films. It is, therefore, important to understand if the magnetic behavior of Mn on surfaces and in thin films is fundamentally different from that in the bulk. For example, do Mn atoms prefer to reside on the surface, do they prefer to cluster, and does the Mn–Mn distance depend upon the crystallographic orientation of the surface? In the following we discuss these aspects.

10.3.1 Mn-doped GaN ($11\bar{2}0$) Surface

We have modeled a thin film having the ($11\bar{2}0$) surface orientation by a nine-layer slab with the supercell [37] containing 72 atoms ($Ga_{36}N_{36}$) as shown in Figure 10.1. To preserve symmetry, the top and bottom layers of the slab were taken to be identical, and each slab was separated from the other by a vacuum region of 10 Å. The central three layers were held fixed at their bulk configuration while the three surface layers on either side of the slab were allowed to relax without any symmetry constraint. *K*-point convergence was achieved with ($6 \times 4 \times 1$) grid, and tests with up to ($8 \times 6 \times 2$) mesh were made.

To study the site preference of a Mn atom, we have first replaced one Ga atom with Mn on the surface layer, the second layer and the third layer on either side of the slab. It was found that Mn atom prefers to reside on the surface site which lies 1.37 and 1.54 eV lower than that of the second and third layer, respectively. This is consistent with the

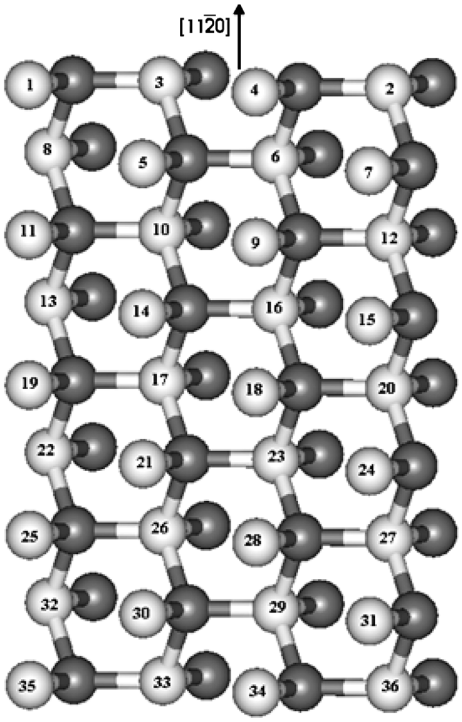

Figure 10.1 Schematic representation of a nine-layer slab model for wurtzite GaN ($11\bar{2}0$) surface. The numbered spheres are Ga

Table 10.1 Relative energies (E_{FM} and E_{AFM}) with respect to the ground state for the $Ga_{32}Mn_4N_{36}$ supercell. ΔE is the energy difference between AFM and FM states ($\Delta E = E_{AFM} - E_{FM}$)

Configuration	E_{EF} (eV)	E_{AFM} (eV)	ΔE (eV)
I (1,3/35,33)	0.403	0.000	−0.403
II (2,3/36,33)	1.722	1.694	−0.028
III (3,4/33,34)	1.773	1.708	−0.065
IV (3,6/33,29)	2.550	2.465	−0.085
V (5,6/30,29)	3.438	3.226	−0.212

experimental finding where Mn atoms doped in GaN were found to migrate to the surface site upon annealing.

The magnetic coupling between Mn atoms was studied by replacing two Ga atoms with Mn on either side of the slab. This amounts to a supercell consisting of $Ga_{32}Mn_4N_{36}$. There are many ways to reach this replacement. We have considered five different configurations, which have been specified in Table 10.1. Geometry optimization and total energy calculation were carried out. We found that configuration I with AFM coupling between Mn atoms is the lowest energy configuration and the FM state is 0.40 eV higher in energy than the AFM state. Other configurations are also AFM and are much higher in energy relative to the ground state. This indicates that Mn atoms couple antiferromagnetically in GaN $(11\bar{2}0)$ thin film.

The total densities of states (DOS) and partial DOS of Mn atom for $Ga_{32}Mn_4N_{36}$ slab with and without geometry optimization are shown in Figure 10.2. For the unrelaxed surface, the coupling is FM, the DOS exhibits half-metallic behavior similar to that in (Ga, Mn)N crystal. When the surface is fully optimized, the coupling becomes AFM and the spin-up and spin-down DOS are identical as the total moment of the system is zero. The magnetic moment at each of the Mn site is found to be 3.0 μ_B with opposite spin orientation. The main contribution to this moment comes from the Mn 3d electrons as can be seen from the partial DOS for the Mn atom in Figure 10.2(c). The hybridization between N 2p and Mn 3d reduces the magnetic moment as compared with that of a free Mn atom. As discussed above, the magnetic coupling between Mn atoms in the crystal is not affected by the relaxation of the structure. However, the situation is different in the surface case. If the surface is not relaxed, the coupling is FM, which becomes AFM upon relaxation.

To understand the physics involved, we checked the changes in bond lengths. Due to relaxation, the bond lengths near the film surface

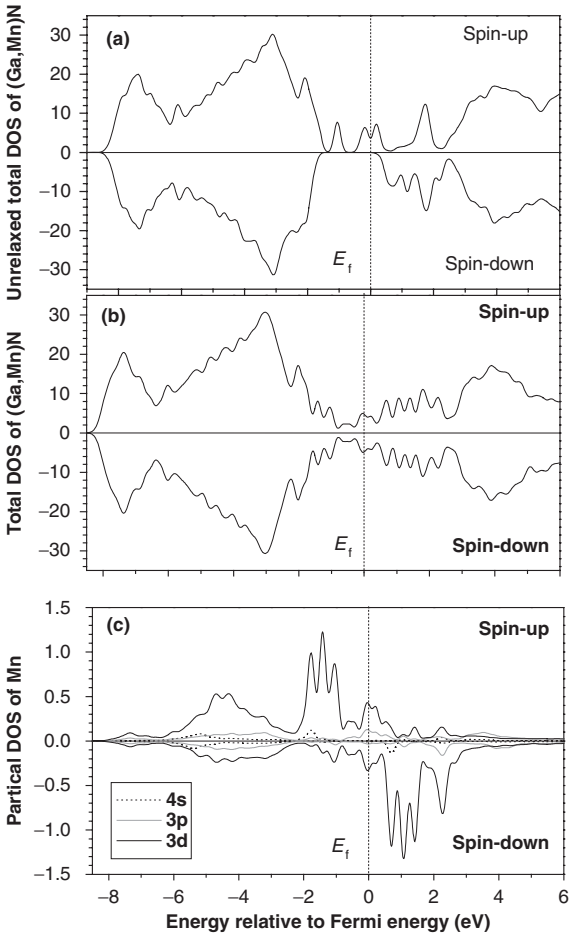

Figure 10.2 Total DOS for (a) an unrelaxed (FM) and (b) a relaxed $Ga_{1-x}Mn_xN$ (AFM). The corresponding partial DOS of Mn atom are shown in (c)

layers are contracted. For example, in the ground state the bond lengths of Mn–N (1.822 Å) and Mn–Mn (2.978 Å) in the first surface layer are significantly shorter than the corresponding bulk values (1.990 and 3.233 Å, respectively). In the second layer the bond lengths of Mn–N and Mn–Mn are 1.920 and 3.093 Å, respectively. In the third layer, they are 1.951 and 3.111 Å, respectively. We see that the bond length contraction mainly occurs in the first two layers, and the magnetic couplings become AFM. Therefore, we can expect an evolution from AFM to FM coupling when Mn atoms diffuse from the surface to the film interior, as the bond length contraction vanishes gradually. However, energetically this is not

preferred and it has been observed experimentally that Mn atoms diffuse from the film interior to its surface.

We note that in the above (1 × 2) (11$\bar{2}$0) surface slab model, the Mn atoms on the surface form a continuous zigzag chain along the [0001] direction. One may wonder if the magnetic coupling results from the formation of these Mn–Mn chains on the surface and if there is an interaction between the impurity atom and its image in the nearest supercell. To clarify this point, we generated a (2 × 2) seven-layer GaN (11$\bar{2}$0) slab containing 56 Ga atoms and 56 N atoms, in which the minimum distance between the impurity atom and its image in the nearest supercell is larger than 10 Å along the [0001] direction. When two Mn atoms are substitutionally doped at Ga sites on either side of the slab, a $Ga_{52}Mn_4N_{56}$ supercell with a 7.14 % Mn concentration is formed. Following the same procedure as described above for the (1 × 2) nine-layer slab, the geometry of the supercell was optimized fully by using (5 × 5 × 1) Monkhorst–Pack *k*-point mesh. Again, the AFM state is found to be more stable than the FM state with an energy difference of 0.06 eV per Mn atom. The Mn–N bond length on the surface layer is 1.82 Å, and the Mn–Mn distance is 2.91 Å. Thus it is clear that the AFM coupling in the thin film is due to bond length contraction, which is insensitive to Mn concentration or the construction of the GaN supercell.

10.3.2 Mn-doped GaN (10$\bar{1}$0) Surface

In order to study if the magnetic coupling between Mn atoms depends upon the orientation of the thin film surface, we have considered (Ga, Mn)N thin film having wurtzite structure and [10$\bar{1}$0] orientation [38]. Note that the Mn–Mn distances may depend upon the surface orientation and hence may affect the magnetic ordering between them.

The GaN (10$\bar{1}$0) surface was modeled by a (2 × 2) 10-layer slab that contains 40 Ga atoms and 40 N atoms in the supercell (Figure 10.3). Each slab was separated from the other by a vacuum region of 10 Å in the [10$\bar{1}$0] direction. The central four layers of the slab were held at their ideal bulk position while the three layers on either side of the slab were allowed to relax without any symmetry constraint. To study the magnetic coupling between the Mn atoms in the GaN (10$\bar{1}$0) thin film, we again substituted two Ga atoms with two Mn on both top and bottom sides of the $Ga_{40}N_{40}$ slab. Consequently, a total replacement of four Ga atoms with Mn results in a 10.00 % Mn doping concentration and a $Ga_{36}Mn_4N_{40}$ supercell. We have considered six different configurations to simulate the different Mn–Mn distance and Mn-N-Mn bond

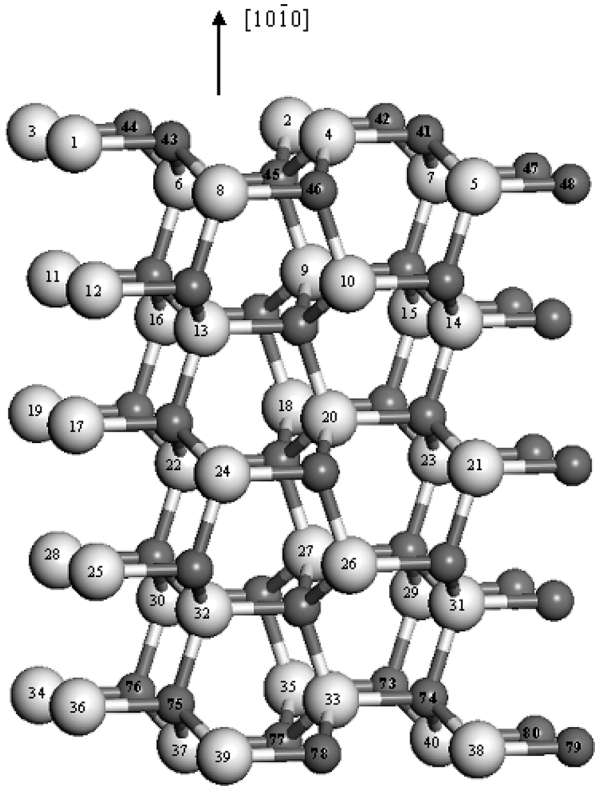

Figure 10.3 Supercell of a 10-layer slab for GaN (10$\bar{1}$0) surface. The larger and lighter spheres are Ga

angle. We have specified the six configurations in the first column of Table 10.2 by giving the sites where the Ga atoms are replaced by Mn (Figure 10.3).

The calculations of total energies and forces, and optimizations of geometry have been carried out the same way as described above for the (11$\bar{2}$0) surface. The main results are summarized in Table 10.2. It is found that configuration I is the ground state with the AFM coupling lying 0.541 eV lower in energy than the FM one, where the two Mn atoms reside on the surface layer sites, and cluster around N atoms. The optimized Mn–N bond length along the [0001] direction is 1.798 Å, corresponding to a contraction of −2.6 % as compared with that for the undoped GaN surface. The Mn–Mn distance of 3.189 Å, however, is unchanged from the corresponding Ga–Ga distance in the undoped case. Comparing the relative energies, we note that the total energy increases as the Mn atoms move from surface layer to the interior sites of the film. Configurations

Table 10.2 The Relative energy ($\Delta\varepsilon$) calculated with respect to the ground state (configuration I), the energy difference (ΔE) between the AFM and FM states ($\Delta E = E_{AFM} - E_{FM}$), the optimized bond length between Mn and its nearest neighboring N ($d_{Mn\text{-}N}$) along the [0001] direction, and the optimized distance between the two Mn atoms ($d_{Mn\text{-}Mn}$) for $Ga_{36}Mn_4N_{40}$

Configuration	$\Delta\varepsilon$ (eV)	ΔE (eV)	Coupling	d_{Mn-N} (Å)	d_{Mn-Mn} (Å)
I (2,4/38,40)	0	−0.541	AFM	1.798(−9.65%)	3.189
II (1,4/37,40)	1.084	0.096	FM	1.813(−8.89%)	5.185
III (1,2/37,38)	1.178	0.002	FM	1.816(−8.74%)	6.087
IV (4,8/40,35)	1.795	−0.047	AFM	1.835(−7.79%)	2.969
V (6,8/33,35)	2.307	0.113	FM	1.973(−0.85%)	3.189
VI (9,10/32,30)	3.228	0.084	FM	1.975(−0.75%)	3.189

V and VI, where the two Mn atoms occupy, respectively, the subsurface and the third layer sites, are found to be 2.307 eV and 3.228 eV higher in energy than the ground state, respectively. This shows again that Mn atoms prefer the surface sites and this site preference is not affected by the Mn concentration. Meanwhile, it is interesting to note that although the Mn–Mn distances in configurations I, V and VI have the same value ($d_{Mn\text{-}Mn} = 3.189$ Å), their corresponding Mn–N bond lengths are quite different, namely 1.798, 1.973, and 1.975 Å respectively, and the magnetic couplings between the Mn atoms in these configurations are also different, i.e. the Mn atoms couple ferromagnetically in configurations V and VI. The coupling in configuration I, however, is AFM. This demonstrates that at certain Mn–Mn distance, the contraction of Mn–N bond length plays a critical role in driving the AFM coupling between the Mn atoms. This is in agreement with the results obtained in the calculations on the $(11\bar{2}0)$ slab.

The total DOS for the ground state configuration I, and the corresponding partial DOS of Mn atom and the partial DOS for Mn 3d and N 2p are plotted in Figure 10.4. We note that the total DOS for spin-up and spin-down are identical leading to zero magnetic moment. The magnetic moment on each Mn atom is $3.05\mu_B$ and mainly comes from the Mn 3d orbital ($2.95\mu_B$). Small contributions to the moment also arises from the Mn 3p ($0.03\mu_B$) and Mn 4s ($0.1\mu_B$) orbitals due to the sp and d hybridization, as shown in Figure 10.4(a_2). The neighboring N atom of Mn is polarized antiferromagnetically with a magnetic moment of $0.06\mu_B$ which mainly comes from N 2p orbitals ($0.05\mu_B$) [Figure 10.4(a_3)].

To study the effect of the Mn concentration on the magnetic coupling between the Mn atoms, we performed extensive calculations on the GaN slabs with different thickness along the $[10\bar{1}0]$ direction, as well as the

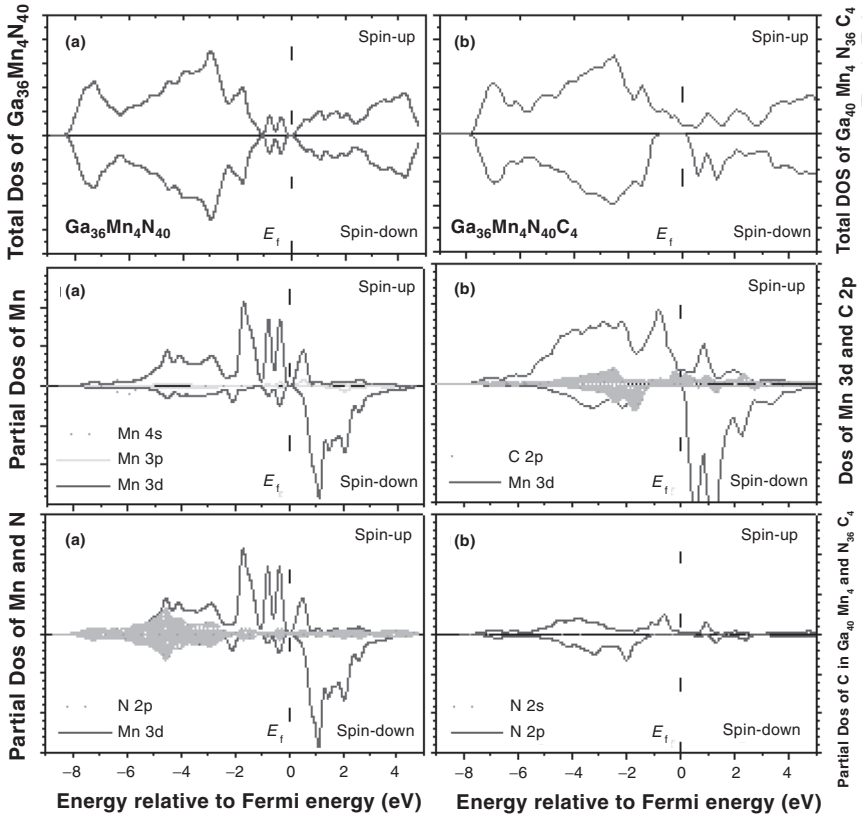

Figure 10.4 (a_1) Total DOS, (a_2) partial DOS of Mn, and (a_3) partial DOS of Mn 3d and neighboring N 2p for $Ga_{36}Mn_4N_{40}$ supercell. (b_1) Total DOS, (b_2) partial DOS of Mn 3d and neighboring C 2p, and (b_3) partial DOS of N for C codoped $Ga_{36}Mn_4N_{36}C_4$ supercell

[01$\bar{1}$0] direction. At first, we increased the thickness of the slab to twelve layers based on the above (2 × 2) 10-layer slab along [10$\bar{1}$0] direction to reach a lower Mn doping concentration. We have also replaced two of the Ga atoms with Mn on either side of the slab, corresponding to a 8.30 % Mn doping concentration. It was found that the configuration where the Mn atoms occupy the nearest neighbor Ga sites on the surface layer is again the ground state with the AFM state being 0.535 eV lower in energy than the FM state. We then performed the calculations for the Mn-doped (2 × 2) eight-layer slab ($Ga_{28}Mn_4N_{32}$) to reach a larger Mn concentration. The ground state is once again found to be AFM with both the Mn atoms residing on the nearest neighbor Ga sites of the surface. The AFM state is 0.549 eV lower in energy than the FM state.

We also performed calculations by changing the Mn concentration by increasing the slab thickness along the $[01\bar{1}0]$ direction. We used a (5×2) six-layer slab containing 60 Ga atoms and 60 N atoms, in which the minimum distance between the Mn atom and its image in the nearest supercell is 10.07 Å along the $[01\bar{1}0]$ direction. In this way, no Mn–Mn chain can be formed along the $[01\bar{1}0]$ direction, and no interaction between the Mn atom and its image can occur. When two Mn atoms are substitutionally doped at Ga sites on either side of the slab, a $Ga_{56}Mn_4N_{60}$ supercell with a 6.70 % Mn concentration is formed. We have carried out extensive search for the most favorable geometric and magnetic configuration. Once again, we found that the Mn atoms prefer to reside on the nearest surface Ga sites and couple antiferromagnetically. To further examine the magnetic coupling between Mn atoms in the dilute condition, we have also generated eight-layer, 10-layer and 12-layer (4×2) GaN $(10\bar{1}0)$ slabs. The Mn doping concentrations of 6.25, 5.00 and 4.20% have been achieved by substituting two Ga atoms with Mn on either side of these slabs, respectively. The results are found to be almost the same as those given in the smaller slabs; namely, the ground state is AFM and lies about 0.1 eV per Mn atom lower in energy than the FM state, where the Mn atoms occupy the nearest surface sites of the Ga atoms and form clusters. The Mn–N bond length is about 1.8 Å. The magnetic moment on each Mn atom is about $3\mu_B$. The main results for the ground state configurations corresponding to various slabs are summarized in Table 10.3. Thus, it is clear that in Mn-doped GaN thin films, the AFM ordering at 0 K is energetically favorable, relative to the FM

Table 10.3 Composition of Mn-doped GaN slab, Mn concentration, the energy difference (ΔE) between the AFM and FM states, the magnetic moment on each Mn atom, the optimized nearest Mn–N bond length ($d_{\text{Mn-N}}$) along the [0001] direction, and the optimized Mn–Mn distance ($d_{\text{Mn-Mn}}$) for the supercells that are listed in the first column

System	Slab layers	Mn concentration (%)	ΔE (eV)	Magnetic moment (μ_B)	$d_{\text{Mn-N}}$ (Å)	$d_{\text{Mn-Mn}}$ (Å)
$Ga_{28}Mn_4N_{32}$	(2×2)-8L	12.50	−0.549	3.01	1.799	3.189
$Ga_{36}Mn_4N_{40}$	(2×2)-10L	10.00	−0.541	3.05	1.798	3.189
$Ga_{44}Mn_4N_{48}$	(2×2)-12L	8.30	−0.535	3.05	1.798	3.189
$Ga_{56}Mn_4N_{60}$	(5×2)-6L	6.70	−0.401	3.10	1.794	3.102
$Ga_{60}Mn_4N_{64}$	(4×2)-8L	6.25	−0.422	3.09	1.795	3.095
$Ga_{76}Mn_4N_{80}$	(4×2)-10L	5.00	−0.432	3.09	1.795	3.098
$Ga_{92}Mn_4N_{96}$	(4×2)-12L	4.20	−0.399	3.10	1.794	3.098

L, layer.

state, due to the Mn–N bond length contraction. The magnetic coupling between Mn atoms is insensitive to the concentration of Mn over a wide range of concentration from 4.2 to 12.5 %.

10.3.3 Mn and C Codoped in GaN ($10\bar{1}0$) Surface

We have explored the possibility that the $Ga_{1-x}Mn_xN$ system when codoped with C could turn into a ferromagnet since replacing N with C would introduce hole carriers, which in turn could mediate the FM coupling between the Mn atoms. To this end, we have chosen the 10-layer (2×2) GaN slab codoped with Mn at Ga sites and C at N sites. We calculated the magnetic coupling between Mn atoms following the same procedure as performed for the $Ga_{1-x}Mn_xN$ systems. We replaced respectively one, two and three N with C atoms on either side of the slab, generating corresponding supercells of $Ga_{36}Mn_4N_{38}C_2$, $Ga_{36}Mn_4N_{36}C_4$, and $Ga_{36}Mn_4N_{34}C_6$. For each of these C doping concentrations, we calculated the total energies of various configurations resulting from the replacement of the Ga and N at different sites with Mn and C, respectively. We studied both FM and AFM spin alignments and the effect of full geometry optimization.

When one N atom was replaced with C atom, we found that the ground state configuration is still AFM, in which both the Mn atoms form the nearest neighbor on the surface sites (2, 4) with the C at site 45 binding to both the Mn atoms (Figure 10.3). However, the energy difference between AFM and FM states is considerably reduced (from -0.135 to -0.045 eV per Mn atom). This indicates that a small concentration of C cannot lead to a transition from AFM to FM states.

We, therefore, increased the hole concentration by replacing more N atoms with C on either sides of the slab. For the supercell $Ga_{36}Mn_4N_{36}C_4$, it is interesting to note that for each of the six initial Mn configurations when two N atoms are replaced by C, the ground state is found to be FM, and their corresponding energy differences ΔE between AFM and FM range from 0.03 to 0.08 eV per Mn atom. In Figure 10.5, we plot the energy difference ΔE and the average magnetic moment on Mn atom for the ground states corresponding to the six initial configurations with the C codoping. For comparison, we also plotted the results for the six configurations before C codoping.

The effect of C concentration on the magnetic coupling between Mn atoms was further examined by replacing three N atoms with C at different sites on the either side of the slab. It was found that, in the ground

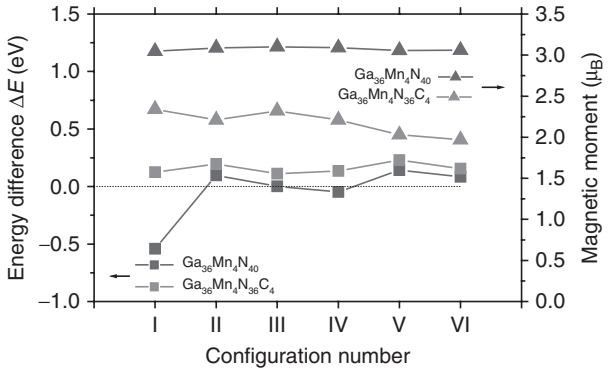

Figure 10.5 Energy difference ΔE between AFM and FM states and the average magnetic moment on Mn atom for the six configurations with and without C codoping. The six configurations are defined in Table 10.3

state configuration where the two Mn atoms reside at sites (2, 4) and C are at sites (41, 42, 45), the FM state is lower in energy by 0.237 eV than the AFM state. Once again, we show that the magnetic coupling between Mn atoms changed from AFM to FM when C is codoped in the $Ga_{1-x}Mn_xN$ system. More importantly, the FM coupling is enhanced by increasing the C concentration, as the energy difference ΔE is increased.

To explore the origin of the FM coupling in C codoped (Ga, Mn)N, we examined the electronic structure corresponding to the ground state configuration of $Ga_{36}Mn_4N_{36}C_4$ supercell and compared it with that for $Ga_{36}Mn_4N_{40}$. The calculated total spin DOS, the partial spin DOS for Mn 3d and C 2p and the partial spin DOS for N atoms in $Ga_{36}Mn_4N_{36}C_4$ are plotted in Figure 10.4(b_1), 4(b_2) and 4(b_3), respectively. Comparing the total DOS in Figure 10.4(a_1) and (b_1), we see that the C codoping has introduced new states near the Fermi level resulting in a half-metallic character of this codoped system. Replacing the group V anion, N, sites with C introduce holes, and electrons are transferred to Mn, which is observed by a strong increase in the Mn^{2+} spin densities at the Fermi level in Figure 10.4(b_1). These induced hole carriers mediate the interaction of the magnetic ions, Mn, resulting in the FM state. As shown in Figure 10.4(a_2), without C codoping, neither Mn nor N introduce DOS at the Fermi energy although there is hybridization between the Mn 3d and N 2p states. However, there is a distinct overlap between Mn 3d and C 2p in the spin-up bands in Figure 10.4(b_2), which leads to new states at the Fermi energy and hence results in a change of the magnetic coupling. Thus, it is clear that the interaction between the localized spins on the

Mn ions and delocalized carriers (holes originating from the C valence band) is responsible for the magnetic transition.

10.4 Mn- AND Cr-DOPED GaN ONE-DIMENSIONAL STRUCTURES

Recently one-dimensional nanostructures consisting of nanowires (NWs), nanotubes (NTs) and nanoholes (NHs) of GaN have been successfully synthesized [39–53]. Because of their unique physical properties and high chemical reactivity and their potential for applications in lasers, transistors, and spintronics devices, these materials have attracted considerable attention. Moreover, their properties can be easily influenced by coating and doping. In particular Mn-doped GaN NWs have been found to be FM up to 300 K [54–57]. Thus, these materials represent an important class of nanoscale building blocks for miniaturized electronic and optical devices. A fundamental understanding of the electronic and magnetic properties of these low dimensional FM semiconductor nanostructures is crucial for the development of spintronics devices. Therefore, we performed a comprehensive theoretical study on the GaN low dimensional nanostructures from first principles to provide an understanding of the experiment and to predict new materials. We used spin polarized density functional theory and different levels of correlation corrections (GGA, LSDA+U and GGA+U) implemented in the VASP code.

10.4.1 Mn-doped GaN Nanowires

We first present our results on the Mn-doped GaN NWs. The GaN NW has been generated from a bulk GaN ($7 \times 7 \times 2$) supercell having the wurtzite structure by removing the outside part of the circled area in Figure 10.6(a) along the [0001] direction [58]. The supercell consists of 96 atoms ($Ga_{48}N_{48}$) and has about 12 Å vacuum space along the $[10\bar{1}0]$ and $[01\bar{1}0]$ directions to prevent the NW from interacting with its image. The NW has 1.0 nm diameter and infinite length along the [0001] direction, as shown in Figure 10.6(b). In Figure 10.7 we show the various sites where Ga atoms were replaced by Mn to study not only their site preference but also how their magnetic coupling depends on the Mn–Mn distance and coordination. For each of these configurations we computed the total energies corresponding to both FM and AFM

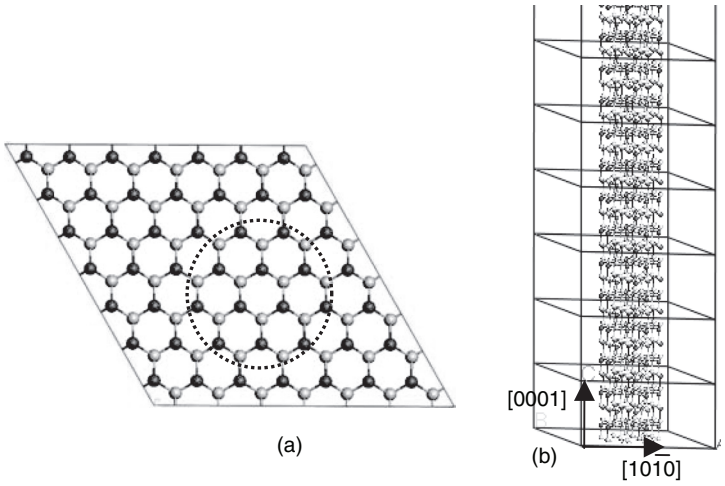

Figure 10.6 (a) Top view of a 7 × 7 × 2 GaN supercell having wurtzite structure. (b) $Ga_{48}N_{48}$ supercell which yields a NW of infinite length along the [0001] direction

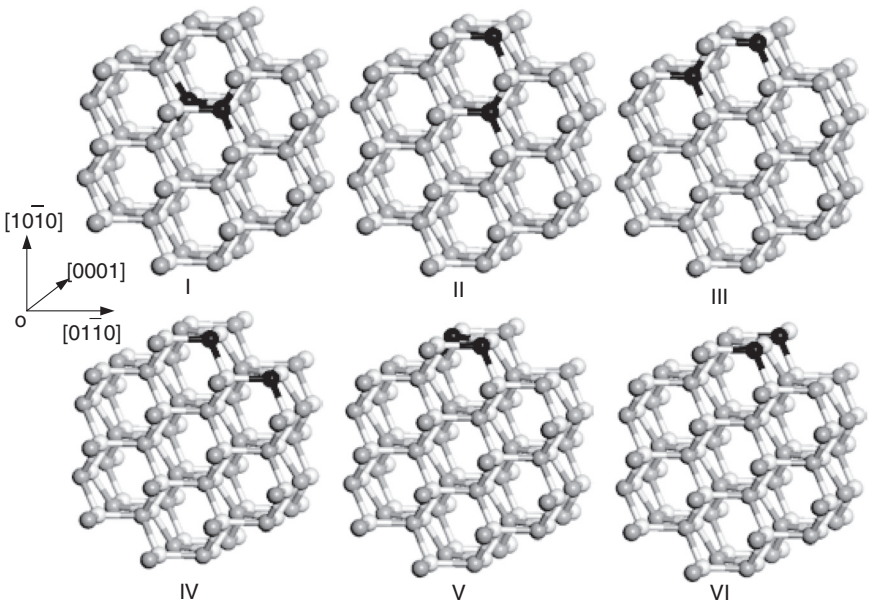

Figure 10.7 Six configurations of $Ga_{46}Mn_2N_{48}$ supercell identifying various Ga sites that have been replaced by Mn. The lighter spheres are N, the grey spheres are Ga, and the black spheres are Mn

Table 10.4 Energy difference (ΔE) between AFM and FM states, the relative energy ($\Delta\varepsilon$) calculated with respect to the ground state (configuration V), the optimized Mn-N ($d_{\mathrm{Mn-N}}$) and Mn-Mn ($d_{\mathrm{Mn-Mn}}$) distances, and the magnetic moments at Mn (μ_{Mn}) and its nearest neighbor N (μ_{N}) atoms for the configurations given in Figure 10.7

Configuration	ΔE (eV)	$\Delta\varepsilon$ (eV)	$d_{\mathrm{Mn\text{-}N}}$ (Å)	$d_{\mathrm{Mn\text{-}Mn}}$ (Å)	μ_{Mn} (μ_{B})	μ_{N} (μ_{B})
I	0.162	1.458	1.913	3.075	3.388	−0.0121
II	−0.363	0.617	1.774	2.755	2.165	−0.05
III	−0.14	0.66	1.818	2.677	2.706	−0.025
IV	0.067	0.191	1.834	3.293	3.194	−0.09
V	0.075	0	1.839	2.965	3.488	−0.114
VI	0.02	0.283	1.837	5.19	3.269	−0.02

alignments of the Mn spins. The atomic coordinates of all the atoms in the supercell were optimized without any symmetry constraint. Results of our calculation are summarized in Table 10.4.

We see that the FM state of configuration V has the lowest energy with its AFM state lying 0.075 eV above the FM state. In this configuration the two Mn atoms reside in the outermost surface sites and form the zigzag chain along the [0001] direction. The next two higher energy configurations (IV and VI) which lie 0.191 and 0.283 eV above the ground state are also FM. For these two configurations the Mn–N distances are nearly the same as that in the ground state configuration, namely 1.84 Å, but the Mn–Mn distances are very different, namely 3.293 and 5.190 Å. This could imply that the Mn–N distance may play a more crucial role than the Mn–Mn distance in dictating the magnetic coupling between the two Mn atoms.

To study the effect of the wire diameter on the magnetic properties of Mn-doped GaN NW, we performed the calculations for the thinnest GaN NW which has been created from a GaN ($5 \times 5 \times 4$) supercell by cutting the part outside of the innermost hexagonal unit along [0001] direction. The corresponding supercell consists of 48 atoms ($Ga_{24}N_{24}$) with a diameter of 0.45 nm. We have also replaced two of the Ga atoms with Mn at different sites to check the magnetic coupling between Mn atoms. It was found that the configuration where the two Ga atoms at the nearest neighbor sites were replaced by Mn is the ground state with the FM state being lower in energy by 0.08 eV than the AFM state, similar to what we found in the previous thicker wire. Therefore, we confirmed that Mn atoms couple ferromangetically, even in such small size GaN NW.

Due to the smaller size of the NW and the large bond length contraction, magnetic moments on Mn sites are small, namely the two Mn atoms only carry magnetic moment of 0.604 and 0.555μ_B. These Mn moments are smaller than any existing values in bulk or thin films. Therefore, in one-dimensional systems the wire thickness can be used to control the magnitude of the magnetic moment.

10.4.2 Cr-doped GaN Nanotubes

The GaN NT has been generated from a (7 × 7 × 3) GaN bulk supercell having wurtzite crystal structure (Figure 10.8) [59]. We removed the atoms from the outside and inside areas of the two circles and replaced them with vacuum space. The NT supercell thus created extends to infinity along the [0001] direction through the repetition of the supercell. This GaN NT has a polygon periphery. The geometry optimization was carried out and it was found that the initial polygon structure transformed into a perfect cylindrical tube with a diameter of 9.84 Å – GaN single wall nanotube (SWNT), as shown in Figure 10.9. It is interesting to note that this optimized SWNT has the same structural feature as the carbon (9, 0) SWNT. To check the structural stability of the GaN SWNT, we performed finite-temperature *ab initio* molecular dynamics calculations. It was found that the tubular structure at $T = 0$ K remains stable at 300 K after 2000 time steps with a time step of 1.0 fs. No significant distortions have been found.

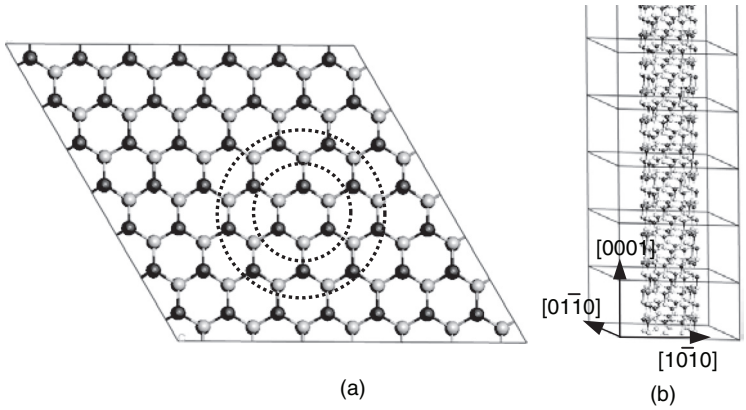

Figure 10.8 (a) Top view of a 7 × 7 × 3 GaN supercell having wurtzite structure. (b) GaN-NT supercell ($Ga_{54}N_{54}$) which extends to infinite length along the [0001] direction

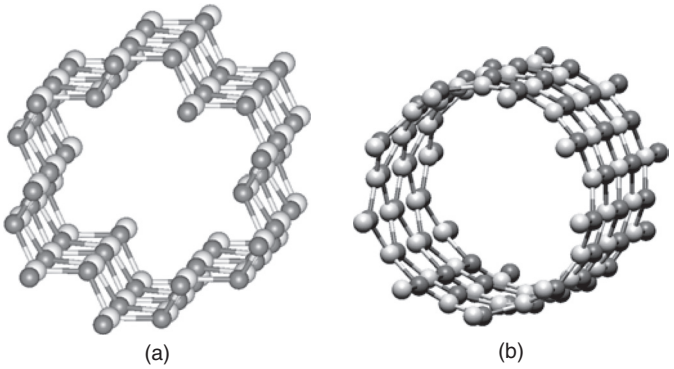

Figure 10.9 Schematic representation of the initial (a) and optimized (b) GaN NT supercell, viewed along the [0001] direction. The lighter spheres are Ga and the darker spheres are N

The preferred site and magnetic coupling between Cr atoms in the GaN NT was studied by carrying out total energy calculations for both FM and AFM configurations and for six different placements of the Cr atoms. We started the calculations with the initial polygonal geometry, since it is not clear if the NT's geometry would change into the SWNT, once Cr is doped. It was found that the initial geometries of all the configurations change substantially following the relaxation. The optimized geometries of all the configurations are tubular with almost the same radius as that of the pure GaN SWNT and similar to that for the carbon (9, 0) SWNT. The configuration with two Ga atoms at nearest neighbor sites on the same (0001) plane was found to be the ground state. The FM state is 0.245 eV lower in energy than the AFM state. The surface relaxation has resulted in a large change of the Cr–Cr distance, from 3.189 to 3.408 Å.

To study the effects of the thickness of the NT wall and the Cr concentration on the magnetic coupling between Cr atoms, we performed additional calculations for a GaN multi-wall nanotube (MWNT). This was generated from a $(9 \times 9 \times 2)$ GaN supercell following the same procedure as discussed for the GaN SWNT. The MWNT supercell contains a total of 192 atoms with a diameter of 7.808 Å for the innermost wall and a diameter of 16.259 Å for the outermost wall. We have replaced a pair of the nearest neighbor Ga atoms with two Cr atoms to study their magnetic coupling. These replacements resulted in four configurations (Figure 10.10), and correspond to a 2.1 % Cr doping concentration ($Ga_{94}Cr_2N_{96}$). It was found that configuration I is the ground state with FM state lying lower in energy by 0.074 eV than that in AFM state. The

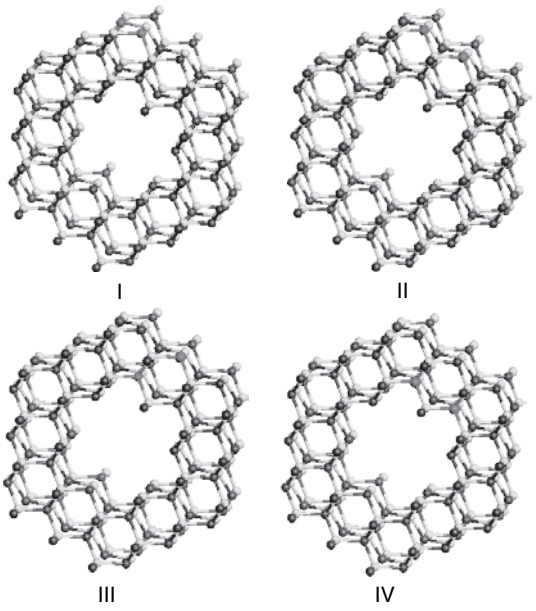

Figure 10.10 Schematic representation of the four configurations of Cr-doped GaN MWNT supercells

other three configurations are respectively 0.214, 0.882 and 1.132 eV higher in energy than the ground state configuration I. Therefore, it is apparent that the FM coupling between the Cr atoms is not affected by the thickness of GaN NT.

To further confirm that the calculated ferromagnetism in Cr-doped GaN NTs is not a consequence of the approximation to exchange and correlation potential, we have employed the LSDA+U method [60, 61]. This replaces the Coulomb interaction among the localized electrons (e.g. transition metal d) by statically screened parameters U and J. We considered the Coulomb correction for Cr 3d electrons in the calculations for the ground state configurations of both the SWNT and the MWNT. We chose the same value for the exchange interaction parameter J, namely, 0.87 eV, which was used in some previous calculations [62, 63] and varied the Coulomb correction U from 2 to 6 eV treating it as a screened parameter. It was found that the FM states are always lower in energy than the AFM states, the introduction of U over a quite large range does not change the magnetic coupling between Cr atoms. This shows the high stability of the FM coupling between Cr atoms in GaN NTs.

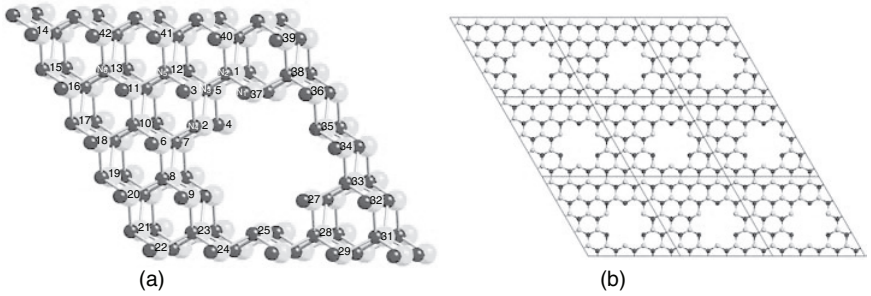

Figure 10.11 Schematic representation of a GaN NH ($Ga_{88}N_{88}$) supercell (a) and GaN NH arrays (b)

10.4.3 Cr-doped GaN Nanohole Arrays

The GaN NH supercell has been generated from a ($5 \times 5 \times 2$) GaN bulk supercell by removing the atoms in a central hexagonal unit along the [0001] direction and replaced with a vacuum space [64]. A supercell containing 88 Ga atoms and 88 N atoms, as shown in Figure 10.11(a), models the NH arrays that extend to infinity through the supercell repetition along the three directions [see Figure 10.11(b)].

To study the magnetic coupling between Cr atoms in the NH, we have again replaced a pair of Ga atoms with Cr at the nearest neighbor sites and at the next nearest sites on the NH surface along different directions to see if clustering of Cr atoms seen in GaN bulk, thin film and NWs still persists in the NH array. To study the effect of curvature of the NH on the site preference of Cr atoms, we created the configurations where one Ga atom at the surface site and another one at the nearest bulk site or two Ga atoms at bulk sites forming the nearest neighbor were replaced with Cr atoms. Total energy calculations with full geometry optimizations were performed for both FM and AFM spin alignments for all the configurations. The configuration with the Cr atoms replacing two Ga at the nearest surface sites in the same (0001) plane was found to be the ground state with the FM state lying 0.128 eV lower in energy than the AFM state. The configurations with the two Cr atoms at the bulk sites and one at bulk site and another at surface are found to be higher in energy by 0.958 and 0.910 eV than the ground state, respectively, which indicates that Mn atoms couple ferromagnetically in the NH, the Cr atoms like to be close to each other and reside on the surface sites of the NH.

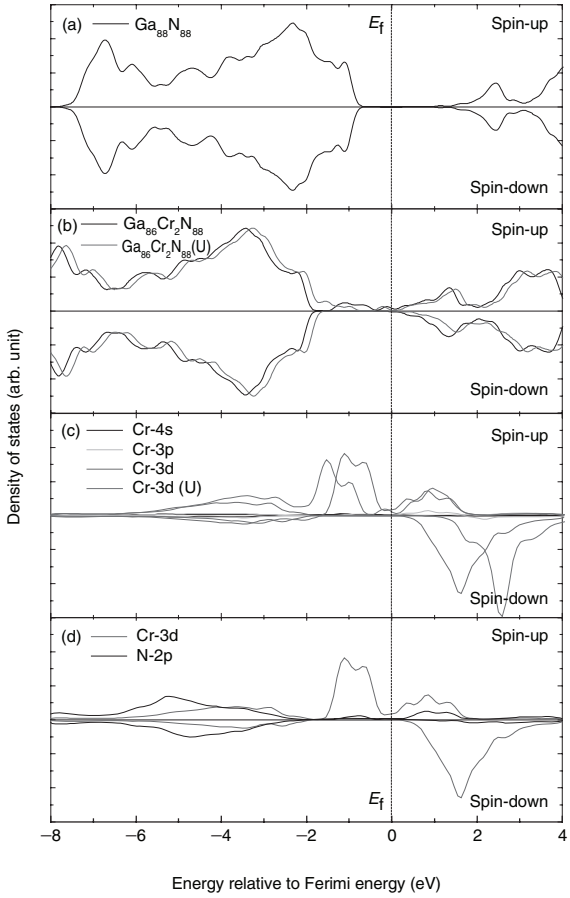

Figure 10.12 (a) Total DOS corresponding to pure $Ga_{88}N_{88}$ NH, (b) total DOS of Cr-doped GaN NH, (c) partial spin DOS of Cr atom, and (d) partial spin DOS of Cr 3d and N 2p in $Ga_{86}Cr_2N_{88}$ supercell

We plot the total DOS and the partial DOS for the NH with and without Cr doping using GGA and GGA+U in Figure 10.12. The total DOS show the semiconductor feature for the pure NH and half-metallic feature for Cr-doped NH. The Cr 3d majority states dominate the total DOS in the band gap region. There is a visible overlap between Cr 3d and N 2p states [Figure 10.12(d)]. The Coulomb correlation effect is obvious: it enhances the gap in the spin-down DOS and the exchange splitting of Cr 3d at the Fermi level. As shown in Figure 10.12(c), there is a downward shift of the Cr 3d spin-up valence states (i.e. the high peak DOS near ~ -1.2 eV shifts down to ~ -1.6 eV from the Fermi energy

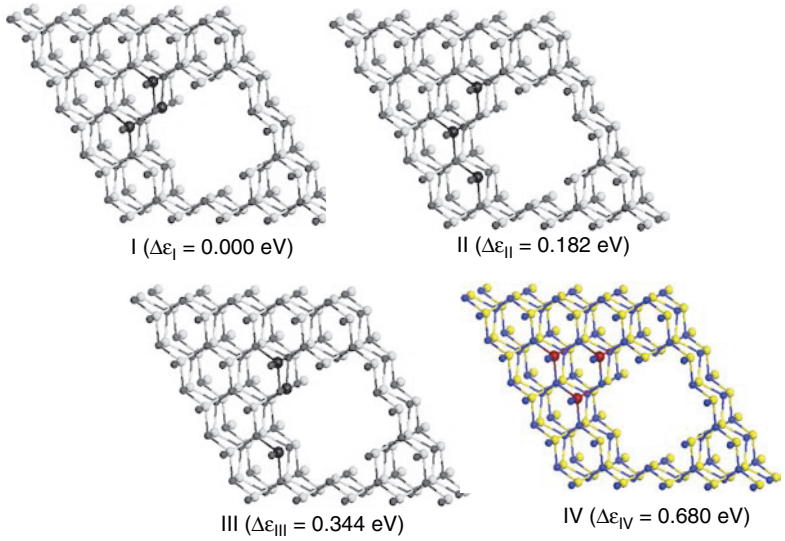

Figure 10.13 Four configurations of $Ga_{85}Cr_3N_{88}$ supercell. The yellow spheres are Ga, the blue spheres are N, and the red spheres are Cr

E_F), and an upward shift of the Cr 3d spin-down conduction states (from ~1.6 to ~2.6 eV away from the E_F).

To further explore the magnetic interaction between the Cr atoms and the effect of Cr concentration on the magnetic coupling between Cr atoms in the GaN NH system, we have performed additional calculations for the configurations where three and four Ga atoms were replaced by Cr in the supercell, corresponding to a slightly higher Cr concentration of 3.4 and 4.5 %, respectively. We have carried out an extensive search for their most favorable geometric and magnetic configurations. Four typical configurations, as shown in Figure 10.13, have specifically been discussed for the case where three Cr atoms were substituted.

For each configuration, calculations were carried out for different spin alignments, namely FM (↑↑↑), and ferrimagnetic (↑↓↑), (↑↑↓), (↓↑↓), (↑↓↓). It was found that the configuration I is the energetically most stable state lying lower in energy by 0.182, 0.344 and 0.680 eV than the other three configurations, respectively. For the ground state configuration, it was found that the (↑↑↓) spin alignment is lower by 0.051, 0.230, 0.192, and 0.221 eV in energy than that for (↑↑↑), (↑↓↑), (↓↑↓), and (↑↓↓), respectively. The total moment for this ground state was found to be $2.775\mu_B$ with each Cr atom carrying a local moment of $(2.274, 2.990, -2.695)\mu_B$. For the case where four Cr atoms were substituted,

the total energy calculations also clearly show that Cr atoms prefer to cluster. The most stable configuration is the one where the four Cr atoms occupy the nearest neighbor sites at the NH surface. For this ground state configuration, calculations were also carried out for different spin alignments, namely (↑↑↑↑), (↑↓↑↓), (↑↓↓↑), (↑↑↓↓), (↓↑↑↑), (↑↓↑↑), (↑↑↓↑) and (↑↑↑↓). It was found that the energetically most favorable spin state again is ferrimagnetic (↓↑↑↑) with a total magnetic moment of 6.863 μ_B. The results indicates that the Cr atoms indeed prefer to cluster in the GaN NH, the preferred magnetic coupling is ferrimagnetic for the Cr cluster larger than two atoms, and the magnetic interaction in the Cr-doped NH is shorted ranged, as found in Cr-doped GaN bulk system [65, 66].

10.5 N-DOPED Mn AND Cr CLUSTERS

From the above study, we note that the clustering of Mn or Cr around N is responsible for the ferromagnetism of Mn- or Cr-doped bulk GaN as well as the large variation in the Curie temperature of different samples. Although Mn and Cr are both AFM in bulk phase, these impurity atoms, when doped into GaN, go to Ga substitutional sites as Cr^{3+} and Mn^{3+} valence states in d^3 and d^4 configurations, respectively, and result in ferromagnetism in Mn- or Cr-doped GaN bulk systems. Note that Mn_4N is known to be FM with a Curie temperature 745 K [67]. This raises the question whether, under suitable growth conditions, Mn-doped in GaN can form Mn_4N clusters. It is, therefore, interesting to examine how Mn_xN clusters form in the gas phase and how their structure evolve with the addition of Mn atoms one at a time.

10.5.1 Giant Magnetic Moments of Mn_xN Clusters

Calculations of the equilibrium geometries, total energies, electronic structure, and magnetic properties have been carried out for Mn_xN clusters for $x = 1$–5 [68]. The geometries are given in Figure 10.14. We found that the binding energy of Mn clusters can be substantially enhanced by N atoms by having their hybridized s-d electrons bond with the p electrons of N. This stabilization is accompanied by FM coupling between the Mn atoms which, in turn, are antiferromagnetically coupled to N atoms. This N mediated FM coupling also gives rise to giant magnetic moments of Mn_xN clusters with total magnetic moments of 4 μ_B, 9 μ_B, 12 μ_B, 17 μ_B, and 22 μ_B for $x = 1$–5, respectively. On the contrary, Mn_x

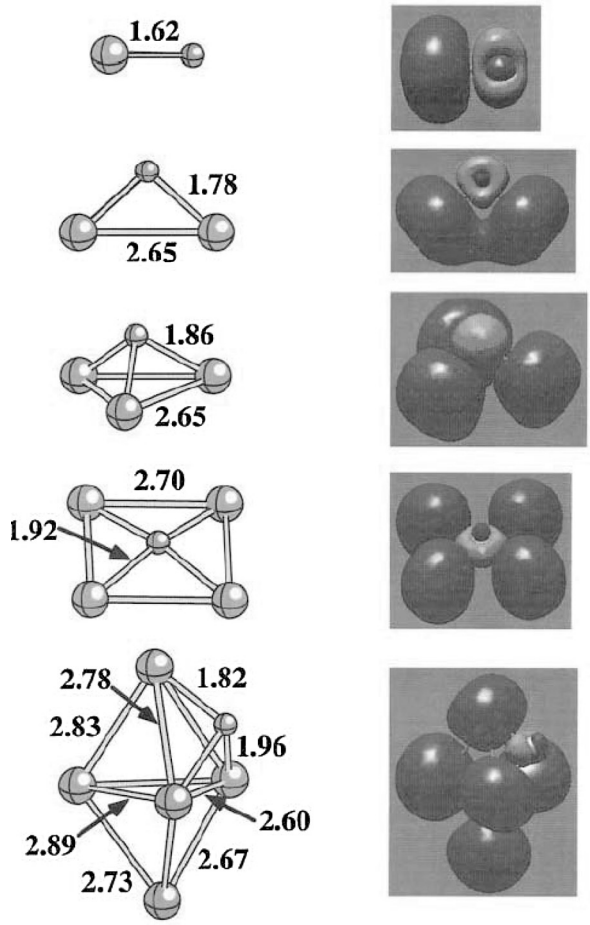

Figure 10.14 Geometries of Mn_xN clusters in their ground states. The bond lengths are given in angstroms. The spin density surfaces corresponding to 0.005 a.u. for these clusters are plotted on the right. The green surfaces represent negative spin densities around the N site while the blue represents positive spin density around Mn sites

clusters are weakly bound and Mn_7 is known to exhibit FM behavior. Thus, study of Mn_xN clusters in the gas phase sheds light on the magnetic properties of Mn-doped GaN.

10.5.2 N-induced Magnetic Transition in Small Cr_xN Clusters

Although Cr and Mn are neighbors in the periodic table, they exhibit very contrasting behavior while sharing some common features. Cr atoms

bind strongly with another Cr atom and the resulting sextuple bonding in a Cr_2 dimer yields a very short bond (1.68 Å) and a large binding energy (1.44 eV). However, Mn_2 is very weakly bonded and has the largest bond length of any dimer in the 3d series. However, both Mn and Cr are AFM in their bulk phase. It is interesting to see if Cr clusters couple ferromagnetically when doped with a N atom, just as Mn_xN clusters have been seen to do [68]. Calculations show that Cr_x clusters are antiferromagnetically coupled with total magnetic moments of 0 μ_B, 6 μ_B, 0 μ_B, and 2 μ_B for $x = 2$–5, respectively, while the doping of N drastically modifies their magnetic properties. Cr_xN clusters are ferromagnetically coupled with Cr atoms coupled antiferromagnetically to the nearest-neighbor N atom. The magnetic moments of Cr_2N and Cr_3N are, respectively, $9\mu_B$ and $13\mu_B$. The binding of N and Cr is substantially larger than that between the Cr atoms. Thus, clustering of Cr atoms around N is energetically favorable in the gas phase.

These observations in N-doped Mn and Cr clusters have relevance to the studies of the observed ferromagnetism in Mn- and Cr-doped GaN, as in these systems, it is possible that Mn and Cr atoms could cluster around N. Therefore, Curie temperatures could be enhanced since it is proportional to the square of the moment. Thus, one can expect that as an impurity (Mn or Cr) in GaN, the giant 'cluster magnets' may play a significant role in the observed ferromagnetism in (Ga,Mn)N or (Ga,Cr)N semiconductors.

10.6 SUMMARY

A comprehensive study of the electronic structure and magnetic properties of the Mn- and Cr-doped GaN has been carried out to study how the dimensionality, local coordination, and symmetry play a role not only on the magnetic moments of transition metal atoms but also on their magnetic coupling. The system we have studied include crystalline bulk, $(11\bar{2}0)$ and $(10\bar{1}0)$ thin films, NTs, NWs, NH arrays, and clusters. Our work has led to the following conclusions: (1) We have shown that the magnetic coupling between transition metal atoms in Mn- and Cr-doped GaN can be altered by selecting the dimensionality of the system. In one-dimensional Mn-doped GaN nanostructures, the special topology of the surface and the confinement of electrons in the radial direction drive the coupling to be FM while in thin films the Mn atoms couple antiferromagnetically. In addition, the magnitude of the magnetic moments can be tuned by changing the size of the nanostructures. The flexibility of both

controlling the magnetic coupling and magnetic moment by choosing the dimensionality and the size of the nanostructures may be useful in practical applications. (2) The magnetic coupling between transition metal (TM) atoms is mediated by the N atom in GaN and is very sensitive to the inter-atomic distance between them as well as between the TM atoms and the nearest N atom. (3) The TM atoms prefer to cluster around the N atoms and in general reside on the surface. (4) The surface relaxations in thin films, NTs, NH arrays, and NWs are large and lead to magnetic coupling that may differ strongly from than in the bulk crystals. (5) Our results on (Ga,Mn)N system codoped with C further suggest that it is possible for the Mn atoms to couple ferromagnetically when the concentration of C is increased beyond a critical limit. This FM coupling is due to the hole carriers introduced by C. The density of states in C codoped (Ga, Mn)N shows half metallic behavior where C introduces states at the Fermi level in the spin-up band. The overlap between Mn 3d and C 2p leads to the change in the magnetic coupling. Our theoretical results explain the origin of the vast disagreement between many experiments as due to sample preparation conditions and demonstrate the key parameters that need to be controlled in order for the transition metal doped GaN to be FM. Porous GaN with tailored pore size has the potential for a spintronics material as it contains large surface area with varying curvature and coordination.

ACKNOWLEDGEMENT

This work was supported by the DURINT program administered by the Office of Naval Research (Dr C. Wood) under Grant N00014-0110715.

REFERENCES

[1] H. Ohno, Science **281**, 951 (1998).
[2] T. Dietl, H. Ohno, F. Matsukura, J. Cibert, and D. Ferrant, Scince **287**, 1019 (2000).
[3] M. L. Reed, M. K. Ritums, H. H Stadelmaier, M. J. Reed, C. A. Parker, S. M. Bedai, and N. A. El-Masry, Mater. Lett. **51**, 500 (2001).
[4] M. L. Reed, N. A. El-Masry, H. H. Stadelmaier, M. K. Ritums, M. J. Reed, C. A. Parker, J. C. Roberts, and S. M. Bedair, Appl. Phys. Lett. **79**, 3473 (2001).
[5] S. Sonoda, S. Shimizu, T. Sasaki, Y. Yamamoto, and H. Hori, J. Cryst. Growth **237**, 1358 (2002).
[6] T. Sasaki, S. Sonoda, Y. Yamamoto, K. Suga, S. Shimizu, K. Kindo, and H. Hori, J. Appl. Phys. **91**, 7911 (2002).

[7] G. T. Thaler, M. E. Overberg, B. Gila, R. Frazier, C. R. Abernathy, S. J. Pearton, J. S. Lee, S. Y. Lee, Y. D. Park, Z. G. Khim, J. Kim, and F. Ren, Appl. Phys. Lett. **80**, 3964 (2002).
[8] J. M. Lee, K. I. Lee, J. Y. Chang, M. H. Ham, K. S. Huh, J. M. Myoung, W. J. Hwang, M. W. Shin, S. H. Han, H. J. Kim, and W. Y. Lee, Microelectron. Eng. **69**, 283 (2003).
[9] P. P. Chen, H. Makino, J. J. Kim and T. Yao, J. Cryst. Growth. **251**, 331 (2003).
[10] S. S. A. Seo, M. W. Kim, Y. S. Lee, T. W. Noh, Y. D. Park, G. T. Thaler, M. E. Overberg, C. R. Abernathy, and S. J. Pearton, Appl. Phys. Lett. **82**, 4749 (2003).
[11] Y. Shon, Y. H. Kwon, Sh. U. Yuldashev, Y. S. Park, D.J. Fu, D. Y. Kim, H. S. Kim, and T. W. Kang, J. Appl. Phys. **93**, 1546 (2003).
[12] T. Kondo, S. Kuwabara, H. Owa, and H. Munekata, J. Cryst. Growth **237**, 1353 (2002).
[13] M. E. Overberg, C. R. Abernathy, S. J. Pearton, N. A. Theodoropoulou, K. T. McCarthy, and A. F. Hebard, Appl. Phys. Lett., **79**, 1312 (2001).
[14] K. Sardar, A. R. Raju, B. Bansal, V. Venkataraman and C. N. R. Rao, Solid State Commun., **125**, 55 (2003).
[15] S. Dhar, O. Brandt, A. Trampert, L. Däweritz, K. J. Friedland, K. H. Ploog, J. Keller, B. Beschoten, and G. Güntherodt, App. Phys. Lett. **82**, 2077 (2003).
[16] S. Dhar, O. Brandt, A. Trampert, K. J. Friedland, Y. J. Sun, and K. H. Ploog, Phys. Rev. B **67**, 165205 (2003).
[17] K. H. Ploog, S. Dhar, and A. Trampert, J. Vac. Sci. Technol. B **21**, 1756 (2003).
[18] M. Zajac, J. Gosk, M. Kamiska, A. Twardowski, T. Szyszko, and S. Podsiado, Appl. Phys. Lett.**79**, 2432 (2001).
[19] K. Ando, Appl. Phys. Lett. **82**, 100 (2003).
[20] T. Graf, M. Gjukic, M. S. Brandt, M. Stutzmann, and O. Ambacher, Appl. Phys. Lett. **81**, 5159 (2002).
[21] S. J. Pearton, C. R. Abernathy, G. T. Thaler, R. M. Frazier, D. P. Norton, F. Ren, Y. D. Park, J. M. Zavada, I. A. Buyanova, W. M. Chen and A. F. Hebard, J. Phys.: Condens. Matter **16**, R209 (2004).
[22] S. E. Park, H.-J. Lee, Y. C. Cho, S.-Y. Jeong, C. R. Cho, and S. Cho, Appl. Phys. Lett. **80**, 4187 (2002).
[23] M. Hashimoto, Y.-K. Zhou, M. Kanamura, and H. Asahi, Solid State Commun. **122**, 37 (2002).
[24] J. S. Lee, J. D. Lim, Z. G. Khim, Y. D. Park, S. J. Pearton, and S. N. G. Chu, J. Appl. Phys**. 93**, 4512 (2003).
[25] H. X. Liu, S, Y. Wu, R. K. Singh, L. Gu, D. J. Smith, N. Newman, N. R. Dilley, L. Montes, and M. B. Simmonds, App. Phys. Lett. **85**, 4076 (2004).
[26] W. Kohn and L. J. Sham, Phys. Rev. **140**, A1133 (1965).
[27] Y. Wang and J. P. Perdew, Phys. Rev. B **44**, 13298 (1991).
[28] G. Kresse and J. Joubert, Phys. Rev. B **59**, 1758 (1999).
[29] G. Kresse and J. Furthmüller, Phys. Rev. B **54**, 11169 (1996).
[30] H. J. Monkhorst and J. D. Pack, Phys. Rev. B **13**, 5188 (1976).
[31] M. van Schilfgaarde and O. N. Mryasov, Phys. Rev. B **63**, 233205 (2003).
[32] K. Sato and H.K. Yoshida, Jpn J. Appl. Phys. **40**, L485 (2001); Semiconductor Sci. Technol. **17**, 367 (2002).
[33] L. Kronik, M. Jain, and J. R. Chelikowsky. Phys. Rev. B, **66**, 041203 (2002).

[34] E. Kulatov, H. Nakayama, H. Mariette, H. Ohta, and Y. A. Uspenskii, Phys. Rev. B **66**, 045203 (2002).
[35] G. P. Das, B. K. Rao, and P. Jena, Phys. Rev. B **68**, 035207 (2003).
[36] Y. L. Soo, G. Kioseoglou, S. Kim, S. Huang, Y. H. Kao, S. Kuwabara, S. Owa, T. Kondo, and H. Munekata, App. Phys. Lett **79**, 3926 (2001).
[37] Q. Wang, Q. Sun, P. Jena, and Y. Kawazoe, Phys. Rev. Lett. **93**, 155501 (2004).
[38] Q. Wang, Q. Sun, and P. Jena, Phys. Rev. B **75**, 035322 (2007).
[39] W. Han, S. Fan, Q. Li, and Y. Hu, Science **277**, 1287 (1997).
[40] G. Cheng, L. D. Zhang, Y. Zhu, G. T. Fei, L. Li, C. M. Mo, and Y. Q. Mao, Appl. Phys. Lett. **75**, 2455 (1999).
[41] X. Duan and C. M. Lieber, J. Am. Chem. Soc. **122**, 188 (2000).
[42] C. C. Tang, S. S. Fan, H. Y. Dang, P. Li, and Y. M. Liu, Appl. Phys. Lett. **77**, 1961 (2000).
[43] Y. X. Chen, S. Ian, I. Stevenson, R. Pouy, L. D.Wang, D. N. McIlroy, T. Pounds, M. G. Norton, and D. E. Aston, Nanotechnology, **18**, 135708 (2007).
[44] J. Y. Li, X. L. Chen, Z. Y. Qiao, Y. G. Cao, and H. Li, J. Mater. Sci. Lett. **20**, 1987 (2001).
[45] J. Goldberger, R. He, Y. Zhang, S. Lee, H. Yan, H. Choi, P. Yang, Nature, **422**, 599 (2003).
[46] S. N. Mohammad, J. Chem. Phys. **125**, 094705 (2006).
[47] T. W. Ebbesen, H. J. Lezec, H. F. Ghaemi, T. Thio, and P. A. Wolff, Nature, **391**, 667 (1998).
[48] M. Law, J. Goldberger, and P. Yang, Annu. Rev. Mater. Res. **34**, 83 (2004).
[49] E. Altewischer, M. P. van Exter, and J. P. Woerdman, Nature, **418**, 304 (2002).
[50] W. L. Barnes, A. Dereux, and T. W. Ebbesen, Nature, **424**, 824 (2003).
[51] P. Andrew, and W. L. Barnes, Science, **306**, 1002 (2004).
[52] T. Thio, H, J. Lezec, T. W. Ebbesen, K. M. Pellerin, G. D. Lewen, A. Nahata, and R. A. Linke, Nanotechnology **13**, 429 (2002).
[53] M. Nebeschuetz, V. Cimalla, O. Ambacher, T. Machleidt, J. Ristic, and E. Calleja, Physica E **37**, 200 (2007).
[54] F. L. Deepak, P. V. Vanitha, A. Govindaraj, and C. N. R. Rao, Chem. Phys. Lett. **374**, 314 (2003).
[55] D. S. Han, J. Park, K.W. Rhie, S. Kim, and J. Chang, Appl. Phys. Lett. **86**, 032506 (2005).
[56] H.-J. Choi, H.-K. Seong, J. Chang, K.-I. Lee, Y.-J. Park, J.-J. Kim, S.-K. Lee, R. He, T. Kuykendall, and P. Yang, Adv. Mater. **17**. 1351 (2005).
[57] C. K. Xu, J. W. Chun, H. J. Lee, Y. H. Jeong, S. E. Han, J. J. Kim, and D. E. Kim, J. Phys. Chem. C **111**, 1180 (2007).
[58] Q. Wang, Q. Sun, and P. Jena, Phys. Rev. Lett. **95**, 167202 (2005).
[59] Q. Wang, Q. Sun, P. Jena, and Y. Kawazoe, Phys. Rev. B **73**, 115411 (2006).
[60] V. I. Anisimov, J. Zaanen, and O. K. Andersen, Phys. Rev. B **44**, 943 (1991).
[61] A. I. Lichtenstein, V. I. Anisimov, and J. Zaanen, Phys. Rev. B **52**, R5467 (1995).
[62] M. A. Korotin, V. I. Anisimov, D. I. Khomskii, and G. A. Sawatzky, Phys. Rev. Lett. **80**, 24305 (1998).
[63] T. Tsujioka, T. Mizokawa, J. Okamoto, A. Fujimori, M. Nohara, H. Takagi, K. Yamaura, M. Takano, Phys. Rev. B **56**, R15509 (1997).
[64] Q. Wang, Q. Sun, P. Jena, and Y. Kawazoe, Phys. Rev. B **75**, 035312 (2007).

[65] X. Y. Cui, J. E. Medvedeva, B. Delley, A. J. Freeman, N. Newman, and C. Stampfl, Phys. Rev. Lett. **95**, 256404 (2005).
[66] L. Bergqvist, O. Eriksson, J. Kudrnovsky, V. Drchal, P. Korzhavyi, and I. Turek, Phys. Rev. Lett. **93**, 137202 (2004).
[67] A. F. Guillermet and G. Grimvall, Phys. Rev. B **40**, 10582 (1989).
[68] B. K. Rao and P. Jena, Phys. Rev. Lett. **89**, 185504 (2002).
[69] Q. Wang, Q. Sun, B. K. Rao, P. Jena, and Y. Kawazoe, J. Chem. Phys. **119**, 7124 (2003).

Au: Where in text?